Available online at www.sciencedirect.com
SCIENCE DIRECT®
Journal of Nuclear Materials 325 (2004) 180–187
journal of nuclear materials
www.elsevier.com/locate/jnucmat

Diffusion reaction between Zircaloy-2 and thoria

P. Sengupta, P.S. Gawde, K. Bhanumurthy, G.B. Kale *

Materials Science Division, Bhabha Atomic Research Centre, Mumbai 400 085, India

Received 30 June 2003; accepted 1 December 2003

Abstract

Diffusion reaction between Zircaloy-2 and thoria (ThO_2) has been studied by employing miniature diffusion couples under uniaxial loading conditions. Electron probe microanalyser (EPMA) has been used to establish the concentration profiles. Microstructural characterisations by scanning electron microscope (SEM) and concentration profiles by EPMA indicate the absence of any intermediate phase in the diffusion zone. The experiments show the preferential grain boundary diffusion of Th and O in Zircaloy-2 matrix. The interdiffusion coefficients are strongly dependent on the temperature of annealing and are of the order of 10^{-18} m^2/s. The activation energy values for the layer growth kinetics and those estimated for interdiffusion coefficients are comparable.

PACS: 66.30.Ny; 66.30.−h; 81.05.Je; 31.70.Hq

1. Introduction

The facts that thorium (Th) can produce U^{233} by (n, γ) reactions and it is more abundant (almost four times) than uranium in earth's crust [1] attracted 'nuclear power programme' planners since long past. Over the last few decades scientists across the world are engaged in introducing 'thorium fuel cycle' in their respective country's 'nuclear power programme'. India has made some progress in this direction and has decided to utilise its vast thorium reserves of 320 000 tonnes [2] for nuclear power generation [3]. As an outcome of this decision, thoria (ThO_2) pellets are to be used as blankets in 'Pressurised Heavy Water Reactors (PHWR)' and 'Fast Breeder Reactors (FBR)' and as a component of 'mixed oxide (MOX) fuel' in 'Advanced Heavy Water Reactor (AHWR)'. ThO_2 is preferred over metallic thorium in nuclear applications for several reasons such as, better irradiation stability, neutron reflectivity and compatibility with coolant. From irradiation performance point of view, performance of thoria based fuels is comparable to or in some cases, better than that of UO_2 on the basis of its structural stability, higher melting point and higher thermal conductivity. It has been noted that thoria based fuels show less structural changes and fission product relocation than UO_2 fuels [4]. To prevent the release of fission products in cooling system thoria pellets are to be cladded with zirconium (Zr) based alloys. In order to understand the interaction between the fuel (ThO_2) and cladding materials (zirconium based alloys) detailed interdiffusion study between these two materials at high temperature is essential. Thoria is added to the zirconia electrolyte of the 'solid oxide fuel cell (SOFC)' to increase the oxygen ion conductivity at high temperature [5,6]. Mutual interaction between Zr and Th is thus important from electrolyte preparation point of view.

The experimental work related to the interdiffusion between metallic thorium and other possible cladding materials are well discussed in the literature [7–9]. Raghunathan et al. [9] have studied the effect of ppm level impurities present in the thorium metal on the diffusion reaction in Th–V system in the temperature range of 1173–1473 K. Bell [7] has investigated the interdiffusion between Th and Zr up to 1173 K and has

* Corresponding author. Tel.: +91-22 2559 5062; fax: +91-22 2550 5239.
E-mail address: gbkale@apsara.barc.ernet.in (G.B. Kale).

0022-3115/$ - see front matter © 2003 Elsevier B.V. All rights reserved.
doi:10.1016/j.jnucmat.2003.12.004

reported negligible reaction between these two metals. Recently Kale et al. [8] have reviewed the interaction of thorium-based fuel with several cladding elements. That report indicated that there is no reaction in the Th–X systems (X = Nb, Ta, Ti, Zr, Mo and V). However, in Th–Al and Th–Mg systems, the metal–metal interactions lead to the formation of several intermetallic compounds. The interdiffusion behaviour of ThO_2 with other metals/oxides is limited [6,10]. Volume and grain boundary diffusion coefficients in ThO_2–$UO_{2.5}$ mixed oxides were evaluated and the transport properties of the mixed oxides were found to be comparable with other mixed oxides [11]. The reaction of ThO_2 pellets with zirconium chloride at 833 K and 923 K has been investigated and results suggested the formation of porous ZrO_2 on the pellets [12]. The diffusion reaction between ThO_2 with the cladding material, Zircaloy-2 is not studied in the literature. The present paper deals with diffusion reaction between ThO_2 and Zircaloy-2 in the temperature range of 1373–1523 K. The objectives of the present work are

(1) to make the diffusion couples between ThO_2 with Zircaloy-2 in a diffusion bonding press under uniaxial load conditions, and
(2) to characterise the microstructure of the interface, to estimate the layer growth parameters and also to evaluate interdiffusion coefficients in ThO_2–Zircaloy-2 system.

2. Experimental work

The diffusion couples were made and annealed in the temperature range of 1373–1523 K and characterised with the help of optical microscope, secondary electron microscope (SEM) and electron probe microanalyser (EPMA). The details of the materials selection, preparation of the diffusion couples, characterisation and analysis of these couples are discussed below.

2.1. Material selection and specimen preparation

Nuclear grade Zircaloy-2 in the form of plate (50 mm × 50 mm) obtained from Nuclear Fuel Complex, Hyderabad were used in these studies. The composition of the Zircaloy-2 is listed in Table 1. Zircaloy-2 pieces of 10 mm × 10 mm have been cut from these plates and annealed at 1173 K for 72 h for grain coarsening.

Table 1
Chemical composition of Zircaloy-2

Element	Fe	Cr	Ni	Sn	Zr
Composition (wt%)	0.12	0.10	0.05	1.50	Balance

Cylindrical thoria (ThO_2) pellets (∅ 10 mm) prepared through oxalate route were used in these studies. Magnesium in the form of 2 wt% $MgSO_4$ was used as a sintering agent and the pellets had been sintered at 1873 K under H_2 atmosphere. The density of these ThO_2 pellets, was about 98% of the theoretical density. The details of the fabrication of ThO_2 pellets are discussed elsewhere [4].

Both Zircaloy-2 and ThO_2 pieces were polished to 1 μm diamond finish by conventional metallographic techniques.

2.2. Preparation of diffusion couples

The diffusion couples were made after placing the polished surfaces of Zircaloy-2 and ThO_2 pieces in contact with each other under vacuum better than 10^{-3} Pa. In order to avoid thermal shock for the ThO_2 pellets the heating rate was kept at 300 K per hour. The specimens were bonded and annealed in the temperature range of 1373–1523 K for 4 h duration. The Zircaloy-2 specimens experienced large deformation during bonding above 1373 K even with dead load of the ram. In order to minimise the deformation, the dead load of the ram was withdrawn during the bonding operation and hence extreme care was necessary for holding the specimens together during the subsequent furnace cooling stage. The diffusion couples thus prepared were mounted and polished perpendicular to the diffusion zone. The zirconium side of the diffusion couples was etched in a solution containing 5 vol.% HF + 45 vol.% HNO_3 + 50 vol.% water. The polished specimens were then observed under optical microscopes to identify the regions for EPMA and SEM studies.

2.3. Electron probe microanalysis

The concentration profiles across the diffusion couples were established using Electron probe microanalyser (CAMECA SX 100). The samples were coated with thin gold layer (~100 Å) for conductivity and then analysed with 20 kV acceleration voltage and 20 nA stabilised beam current. The beam size was kept at $\leqslant 1$ μm to reduce the convolution effect of the beam so as to arrive at a better estimate of the composition across the diffusion zone. Pure zirconium and tin were used as standards for Zr and Sn respectively. Thoria was used as standard for the analysis of Th Mα and O Kα. A standard correction programme based on methods of Pouchou and Pichoir (PAP) [13] was used for atomic number (Z), absorption (A) and fluorescence (F) corrections to obtain true concentrations from the corresponding raw intensity data. The points for analyses were selected at regular intervals of $\leqslant 1$ μm depending

upon the diffusion width by scanning the sample across the bonding interface. In addition, fixed point counting (time $\simeq 100$ s) was employed to estimate the compositions close to the interface.

3. Data analysis

Detailed chemical analyses of the diffusion couples across the interface revealed that the width of the diffusion zone is very small as compared to the width of the parent materials forming the couple thus satisfying the criteria for infinite diffusion couple. Hence Boltzmann–Matano method [14] is used to calculate interdiffusion coefficients from concentration profiles obtained by EPMA. The method involves solution of Fick's second law and interdiffusion coefficient $\widetilde{D}$ at any composition C^* can be given as

$$\widetilde{D}(C*) = -\frac{1}{2t}\left(\frac{\mathrm{d}x}{\mathrm{d}C}\right)\int_{c=c-\infty}^{C*}(x-x_0)\,\mathrm{d}C, \tag{1}$$

with the boundary conditions of $C = C^{-\infty}$ at $x < x_0$, $t = 0$ and $C = C^{+\infty}$ at $x > x_0$, $t = 0$ where 't' is the time of annealing, C^* is any concentration such that $C^{-\infty} < C^* < C^{+\infty}$, '$\left(\frac{\mathrm{d}x}{\mathrm{d}C}\right)$' is the inverse of concentration gradient at C^*, 'x_0' is the position of the Matano interface, $C^{+\infty}$ and $C^{-\infty}$ are the concentrations at the right end and left end of the Matano interface respectively.

4. Results and discussion

4.1. Microstructure of the parent materials

As received ThO_2 specimens were thermally etched at 1823 K for 0.50 h to reveal the microstructure. A typical back scattered electron image (BSE) of sintered ThO_2 pellet is shown in Fig. 1(a). The micrograph shows nearly equiaxed grains with size varying from 20 to 80 μm. As mentioned in the experimental Section (2.1), 2 wt% $MgSO_4$ was used as sintering agent. The X-ray mapping of Th (Mα), O (Kα) and Mg (Kα) are shown in

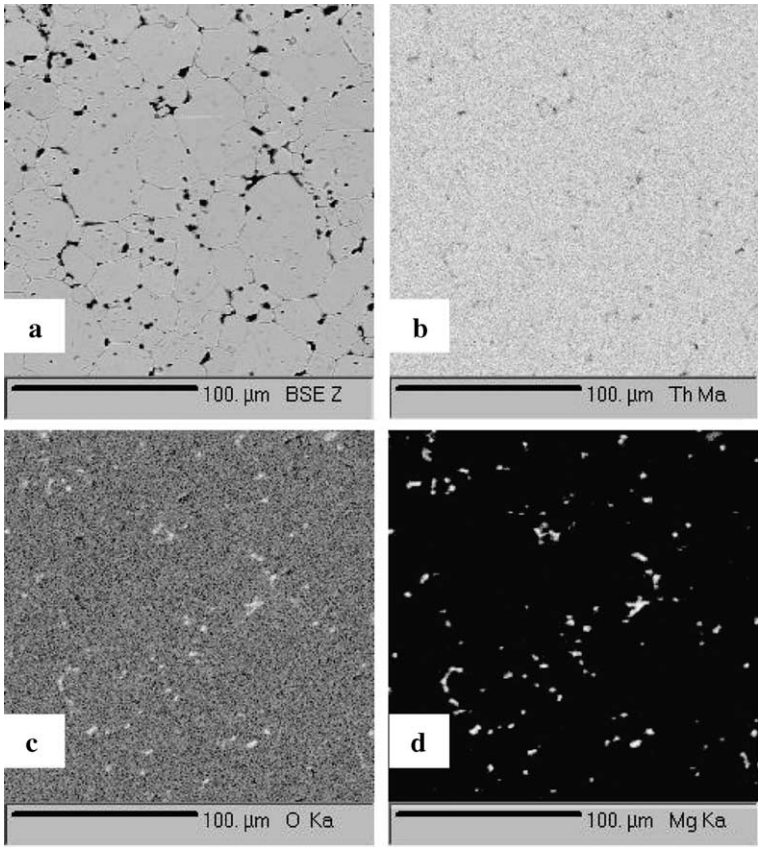

Fig. 1. Microstructure and X-ray images of thoria pellet. (a) BSE image of thoria showing nearly equiaxed grains and the occurrence of magnesia (black precipitates) at the grain boundaries. (b)–(d) X-ray images for Th Mα, O Kα and Mg Kα show the distribution pattern of the elements over the matrix.

Table 2
Phase distribution within thoria pellet by image analysis

Phase	Volume %
ThO_2	93.5
MgO	4.0
Porosity	2.5

Fig. 1(b)–(d) respectively. The X-ray images (Fig. 1(c) and (d)) clearly show the presence of magnesia (MgO), which formed from $MgSO_4$, decorating the grain boundaries. Based on the X-ray mappings, the volume fraction of the magnesia and the porosity are calculated using standard image analysis software and these values are given in Table 2. It can be seen that the volume of the porosity is 2.5%. These results suggest that the density of these pellets is close to the theoretical density. The estimated volume of porosity by image analysis is comparable to the experimentally measured value (2 vol.%).

4.2. Microstructural characterisation of the thoria–Zircaloy 2 interface

A typical BSE image for the diffusion couple annealed at 1573 K for 4 h is shown in Fig. 2 in unetched condition. The micrograph shows good contact between Zircaloy-2 and thoria at the interface. In order to reveal the grain boundaries on the Zircaloy-2 side it was essential to overetch the Zircaloy-2 side of the specimen. Fig. 3 shows the BSE for the same couple in etched condition. It shows good contact with the formation of a black band at the interface due to overetching. The formation of such black band close to the interface has been reported in the heavily etched diffusion couples [15].

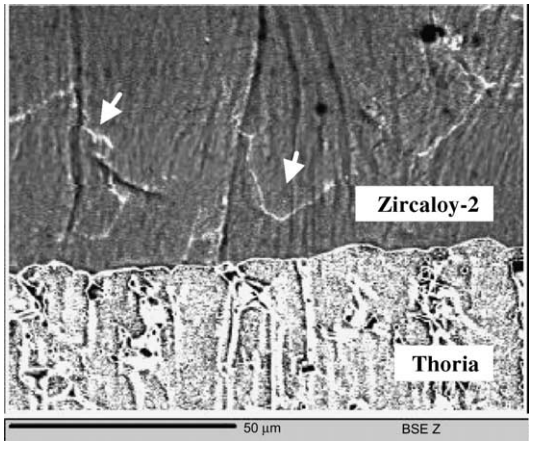

Fig. 2. BSE image of thoria–Zircaloy-2 couple showing good contact at the interface. Arrows indicate grain boundaries enriched in Th and O (see text).

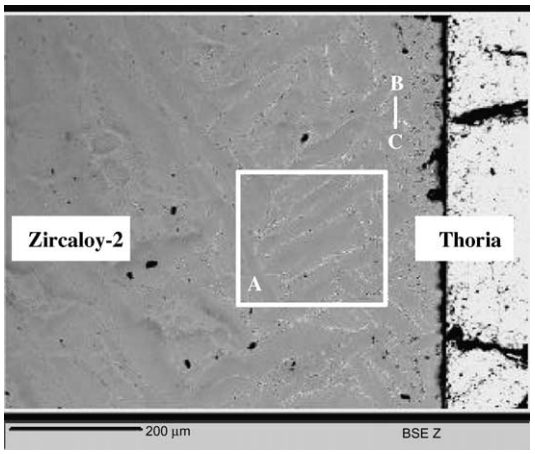

Fig. 3. BSE image of etched diffusion couple (annealed for 4 h at 1573 K) showing the occurrence of transformed α' needles within Zircaloy-2 matrix. X-ray images corresponding to the region marked as A are shown in Fig. 4(a)–(c). B–C represents the line along which X-ray line profiles were taken (Fig. 5).

BSE images taken close to the interface in the diffusion zone on the Zircaloy-2 side (marked as A in Fig. 3) along with the X-ray mappings of Zr (Lα) and Th (Mα) are shown in Fig. 4(a)–(c) respectively. These figures clearly show enrichment of Th and depletion of Zr along the prior β grain boundaries. However, no such enrichment is observed at about 250 μm away from the interface. These results suggest that Th diffuses along β grain boundaries in Zircaloy-2. The enrichment of O (Kα) could not be detected clearly from the X-ray mappings. In order to reveal the behaviour of oxygen, several line scans have been taken across the thorium enriched Zircaloy-2 grain boundaries at different locations. The typical scans for O, Th, and Zr across the grain boundary (along B–C, Fig. 3), which is about 100 μm from the Zircaloy-2 side close to the interface, are shown in Fig. 5. The line scans clearly show the enrichment of Th, O and depletion of Zr along the grain boundary.

The intensity ratios of Th/O (maximum value) are plotted with increase in temperature for several locations from the interface towards Zircaloy-2 and are shown in Fig. 6. It is clear from the figure that the ratio of Th/O increased with increase in temperature at a given distance from the interface and the Th/O intensity ratios decreased with distance at a given temperature (Table 3). The increase in ratio of Th/O with temperature indicates that grain boundary diffusion of Th is faster than that of oxygen. Similar grain boundary diffusion of anion/cation in metal oxides has been reported in NiO [16], CoO [17], Al_2O_3 [18] and ZrO_2 [19]. These studies have shown

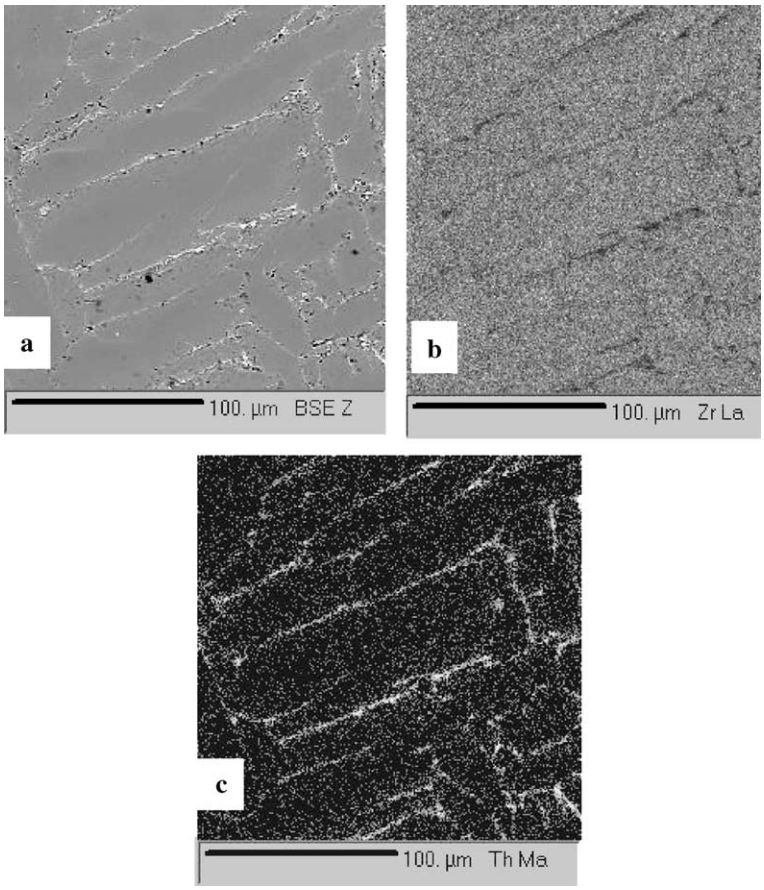

Fig. 4. (a) BSE image, (b) Zr Lα and (c) Th Mα X-ray images taken across the area *A* (see Fig. 3).

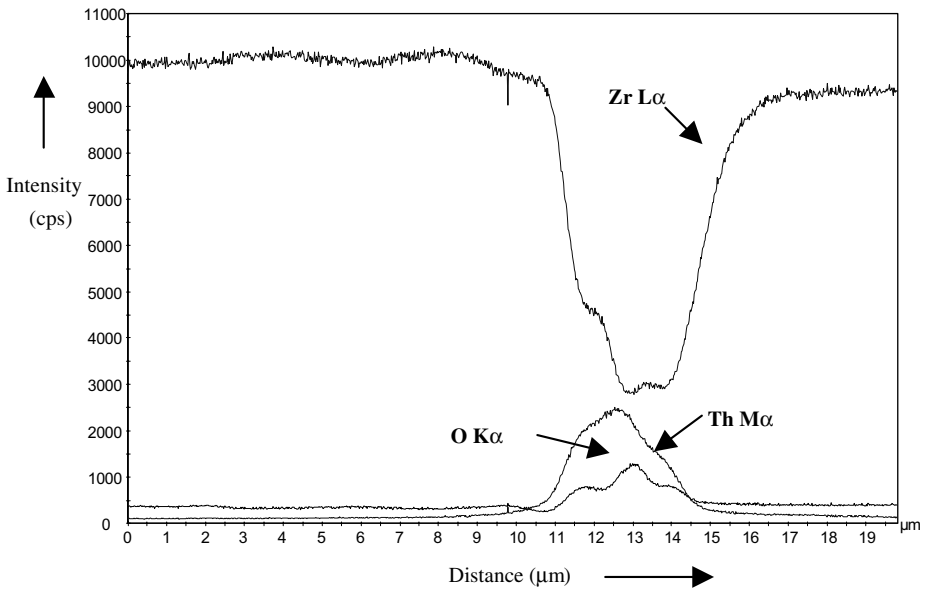

Fig. 5. X-ray line scans for O Kα, Zr Lα and Th Mα taken across the grain boundary (see B–C line, Fig. 3).

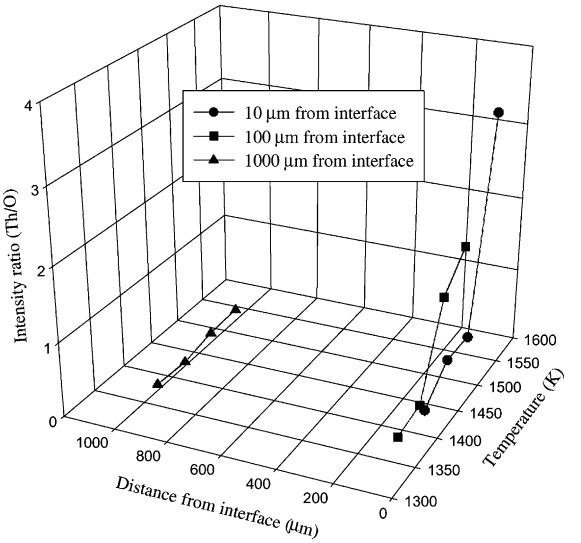

Fig. 6. Three-dimensional plot of Th/O intensity ratios, distance from the interface and annealing temperature.

Table 3
Th/O intensity ratios across the grain boundaries (g.b.)

Temperature (K)	Th/O ratios at different distances from thoria–Zircaloy-2 interface			Th penetration depth along grain boundary (μm)
	10 μm	100 μm	1000 μm	
1373	0.58	0.14	0.09	180
1423	0.89	0.20	0.06	200
1473	0.86	1.33	0.15	220
1523	3.50	1.71	0.17	250

that the transport of cation and oxygen along grain boundaries is faster than that in the bulk phase by several orders of magnitude. No attempts have been made in the present investigation to evaluate the grain boundary diffusion co-efficient. Vieregge and Herzig [20,21] studied the grain boundary diffusion of Zr and Co in polycrystalline α-Zr matrix and reported that they diffuse by different mechanisms. However, based on the present experiments it can be observed that the depth of penetration of O and Th in Zircaloy-2 matrix is much larger compared to the lattice diffusion. The large increase in Th/O ratio at 1523 K also shows that grain boundary diffusion at this temperature is much higher than that at other temperature.

The concentrations of Zr, Th, and O were plotted against the distance for all the diffusion couples to establish the concentration profiles. These profiles showed smooth variation of all the elements indicating the absence of any intermediate phase. The concentration profile of Sn did not indicate any variation in concentration and hence was not recorded. This indicated that it did not diffuse in to thoria side. These profiles were used to evaluate $\widetilde{D}$ values and this aspect is discussed in Section 4.4.

In the absence of Th–Zr–O isotherm at 1523 K in the literature it is rather difficult to comment on the nature of the diffusion path. The binary phase diagrams of Th–Zr, and ThO_2–ZrO_2 [22] show complete solubility. The binary phase diagram of Zr–O system [22] shows that ZrO_2 is the only possible phase. The absence of any thorium rich phase in the diffusion zone commensurates with the Th–Zr and ThO_2–ZrO_2 phase diagrams. Earlier studies on the reaction of ThO_2 with $ZrCl_2$ at 833 and 923 K indicated the formation of adherent but porous ZrO_2 as reaction product on the ThO_2 pellets [12]. However, the present experiments did not show the formation of ZrO_2 at the interface. Interaction between metals/ThO_2 at elevated temperature (2073 K) indicated that metals (Ni, Ti, Si and Be) do not reduce ThO_2 [23,24]. In addition, the Ellingum diagram (temperature dependence of Gibbs free energy of formation of oxides ΔG) [25] also confirms that ThO_2 is a far more stable compound than ZrO_2 at the investigated temperature range and hence the possibility of Zr reducing ThO_2 is difficult. Carniglia et al. [26] have observed that the ThO_2 pellets are O deficient over the temperature range of 1273–2173 K for oxygen partial pressure less than 1 atmospheric pressure. It is possible that ThO_2 got partially reduced to Th essentially due to vacuum condition used in the present experiment. The reduced Th along with O must have diffused through the grain boundaries of Zircaloy-2.

4.3. Growth kinetics of diffusion zone

The widths of the diffusion zone have been estimated from the concentration profiles. It is found that diffusion widths increase with increase in temperature. The diffusion process being temperature dependent, the width of diffusion zone varies with it following an Arrhenius type relationship as given below,

$$x = K_0 t^{1/n} \exp(-Q_P/RT), \tag{2}$$

where x is the diffusion width at temperature T, K_0 is the pre-exponential factor, Q_P is activation energy for the phase growth, 'n' is the reaction index and t is time. In case of diffusion dependent phase growth value of 'n' comes very close to 2. The above equation can be written as

$$x = K_0 t^{1/2} \exp(-Q_P/RT). \tag{3}$$

All the couples were isochronically annealed to evaluate K_0 and Q_P. The log value of widths of the diffusion zone are plotted against reciprocal of the

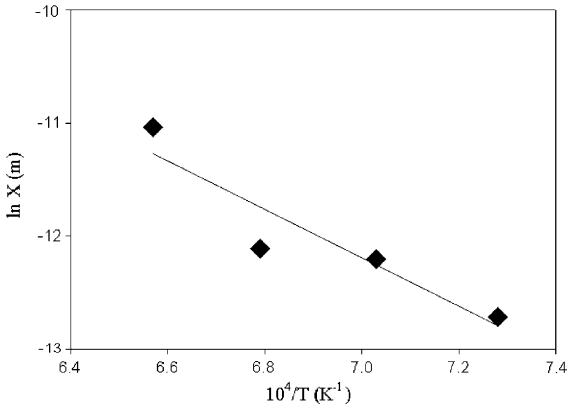

Fig. 7. Temperature dependence of lattice diffusion width for Zircaloy 2/thoria system.

temperature of the diffusion anneal in Fig. 7. The plot is linear as expected from the above relationship. The K_0 and Q_P values have been obtained respectively from the intercept and slope of this graph using least mean square analysis. The values of K_0 and Q_P are 1.15×10^{-7} m/s$^{1/2}$ and 177.9 kJ/g mol respectively. The temperature–time dependence of the diffusion width can be expressed by the following relationship

$$x = 1.15 \times 10^{-7} t^{1/2} \exp(-177.9/RT), \tag{4}$$

where R is expressed in kJ/mol/K. This relation can be used for determining the phase width for a given time of annealing at a given temperature T (K).

4.4. Evaluation of interdiffusion coefficients

The present system is a complex multicomponent system and hence evaluation of diffusion coefficients is rather difficult. Assuming that the interaction is essentially between Th and Zr and neglecting the interaction between O with Zr and Th effective interdiffusion coefficients have been estimated.

The interdiffusion coefficients have been evaluated from the concentration profiles employing Boltzmann–Matano method. The concentration profile of oxygen has not been considered for evaluation of interdiffusion coefficients as it diffuses by interstitial mechanism. As the concentration profiles of Zr and Th are complementary, only the profile of Th has been used for the evaluation of diffusion coefficients. The values of concentrations are fitted with a curve using cubic spline method, and flux is determined by numerical integration as area under the curve, and slope is calculated by numerical differentiation of the profile. The Matano interface has been established using the following the condition

$$\int_{c=c-\infty}^{C+\infty} (x - x_0)\,\mathrm{d}C = 0. \tag{5}$$

The profiles are symmetrical with respect to the Matano interface. The interdiffusion coefficients have been evaluated for various concentrations of Th at various temperatures. The interdiffusion coefficients ($\widetilde{D}$) are plotted against the concentration of Th (Fig. 8). It is seen that these values are of the order of 10^{-18} m^2/s. It can also be noted that $\widetilde{D}$ do not change substantially with increase in Th concentration at lower temperature. However, at 1523 K significant concentrations dependence of $\widetilde{D}$ is observed. The concentration dependence of $\widetilde{D}$ is consistent with Zr–Th phase diagram. The T_s (solidus temperature) decreases with increase in concentration of Th, and accordingly $\widetilde{D}$ increases with concentration of Th.

The temperature dependence has been established by plotting log values of $\widetilde{D}$ at various concentrations against the reciprocal of the temperature of diffusion anneal. The typical temperature dependence for concentration 3.3 at.% Th and 23.1 at.% are shown in Fig. 9. The plots are non-linear in nature. Excluding the points corresponding to 1523 K temperature, the rest of the plots are linear following the Arrhenius relationship. The values of pre-exponential factor D_0 and activation energy Q have been calculated from the intercept and slopes of these plots and are tabulated in Table 4. The similarities of the plots indicate that the activation energies are nearly same for all the concentrations. The activation energy values for interdiffusion are comparable with those for growth of diffusion zone. The activation energy values expressed in joules are of the order of 60 T_m (much less than 142 T_m required for normal diffusion) where T_m is melting point in K. This suggests that interdiffusion in Zr–Th system is anomalous in nature. The values of D_0 are also lower than the values for normal diffusion.

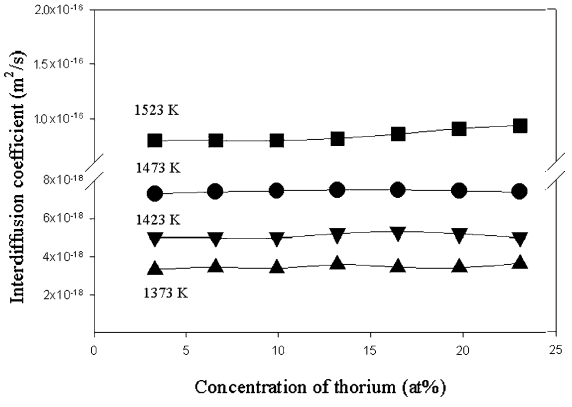

Fig. 8. Concentration dependence of interdiffusion coefficients in Zircaloy-2/thoria system.

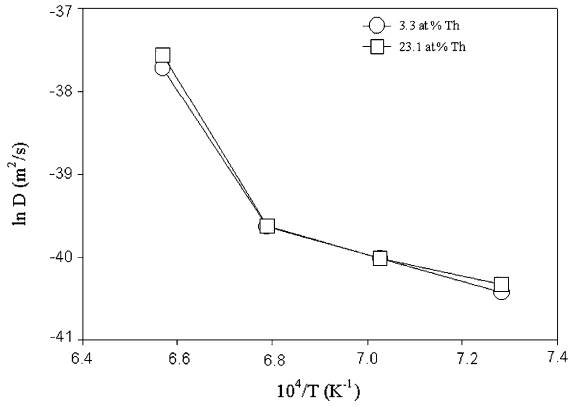

Fig. 9. Temperature dependence of interdiffusion coefficients in Zircaloy-2/thoria system.

Table 4
Pre-exponential factors and activation energies for interdiffusion in Zircaloy-2/thoria system at various concentrations of Th

Concentration of Th (at.%)	Pre-exponential factor ($D_0 \times 10^{13}$ m^2/s)	Activation energy (Q kJ/g mol)
3.30	2.96	132.07
9.90	2.93	131.81
16.50	2.62	130.12
23.10	0.95	118.24

5. Summary and conclusion

From the present diffusion reaction study for Zircaloy–2/thoria system within the temperature interval of 1373–1523 K the following observations can be made,

(1) Th diffuses in Zircaloy-2 through lattice diffusion as well as through grain boundaries.

The lattice driven diffusion layer growth kinetics can be expressed as $x = 1.15 \times 10^{-7} t^{1/2} \exp(-177.9/RT)$ where R is expressed in kJ/mol K.

(2) The interdiffusion coefficients in this system are of the order of 10^{-18} m^2/s.

The interdiffusion coefficients are nearly concentration independent up to 1523 K. At 1523 K, $\tilde{D}$ increases with concentration of Th.

(3) The activation energy values for interdiffusion are in the order of 118–130 kJ/g mol and are comparable with that obtained from growth of diffusion zones.

(4) The interdiffusion of Zircaloy-2/thoria is anomalous in nature.

(5) Th and O diffuse through grain boundaries in Zircaloy-2.

Acknowledgements

The authors are grateful to Dr S. Banerjee, Director, Materials Group, Dr P.K. De, Head, Materials Science Division and Dr P. Mukhopadhyay, Head, Physical Metallurgy Section, BARC for their keen interest in the work.

References

[1] R.D. Nininger, Minerals for Atomic Energy, D. Van Nost, New York, 1955, p. 16.
[2] P. Rodriguez, C.V. Sundaram, J. Nucl. Mater. 100 (1981) 227.
[3] R. Chidambaram, in: M. Srinivasan, I. Kimura (Eds.), Proceedings of the Indo-Japan Seminar of Thorium Utilization, Bombay, 1990, Indian Nuclear Society, and Atomic Energy Society of Japan, p. 7.
[4] M.R. Nair, U. Basak, R. Ramachandran, S. Majumdar, Trans. Powder Met. Assoc. India 26 (1999) 53.
[5] S.P.S. Badwal, K. Foger, Mater. Forum. 21 (1997) 187.
[6] P. Sriramamurti, Thorium fuel cycle development activities in India, BARC Rep. 1532 (1990) 35.
[7] I.P. Bell, Nucl. Eng. 2 (1957) 416.
[8] G.B. Kale, R.V. Patil, in: Proceedings of INSAC 2000, Mumbai, 2000, p. 1.
[9] V.S. Raghunathan, R.V. Patil, S.K. Khera, B.D. Sharma, Met. Trans. 5 (1974) 1141.
[10] W.D. Kingery, H.K. Bowen, D.R. Uhlman, Introduction to Ceramics, Wiley, New York, 1970.
[11] D.R. Olander, J. Nucl. Mater. 144 (1987) 105.
[12] J.A. Kateley, M.J. Tschetter, P. Chiotti, J. Less Commun. Met. 26 (1972) 145.
[13] J.L. Pouchou, F. Pichoir, Microbeam Analysis, San Francisco, California, 1985, p. 104.
[14] C. Matano, Jpn. Phys. 8 (1933) 109.
[15] G.B. Kale, K. Bhanumurthy, K.C. Ratnakala, S.K. Khera, J. Nucl. Mater. 138 (1986) 73.
[16] M. Dechamps, F. Barbier, Non-Stoichiom. Compd. (1984) 221.
[17] K. Kowalski, E.G. Moya, J. Nowotny, J. Phys. Chem. Solids 57 (1996) 153.
[18] E.G. Moya, Science of Materials Interfaces, Elsevier, Amsterdam, 1993, p. 227.
[19] T. Bak, J. Nowotny, K. Prince, M. Rekas, C.C. Sorrell, J. Am. Ceram. Soc. 85 (2002) 2244.
[20] K. Vieregge, C. Herzig, J. Nucl. Mater. 173 (1990) 118.
[21] K. Vieregge, C. Herzig, J. Nucl. Mater. 175 (1990) 29.
[22] T.B. Massalski, Binary alloy and phase diagrams, ASM Int. 3 (1990) 3488.
[23] F.H. Norton, W.D. Kingery, A.E.C. Techn. Information Service, Oak Ridge, Tenn.
[24] E. Ryshekewitch, Oxide Ceramics, Academic Press, New York, 1960, p. 417.
[25] F.D. Richardson, J.H.E. Jeffes, Iron J. Steel Inst. 106 (1948) 261.
[26] S.C. Carniglia, S.D. Brown, T.F. Schroeder, J. Am. Ceram. Soc. 54 (1971) 13.